Biocatalysis and Agricultural Biotechnology 21 (2019) 101352

Contents lists available at ScienceDirect

Biocatalysis and Agricultural Biotechnology

journal homepage: http://www.elsevier.com/locate/bab

Environmental pollutants simultaneous determination: DNA catalyst mediated polyaniline biocomposite nanostructures

P. Thivya, Wilson R. Ramya J.*

Polymer Electronics Lab, Department of Bioelectronics and Biosensors, Alagappa University, Karaikudi, 630 004, Tamilnadu, India

ARTICLE INFO

Keywords:
Polyaniline
MoS_2
Hydroquinone
Catechol
Resorcinol
Nitrite
DNA

ABSTRACT

In this work, α-Fe_2O_3, Polyaniline (PANi), MoS_2 sheets and DNA are integrated as a versatile platform by a simple chemical route for the detection of environmental pollutants. The structure and morphology of the hybrid characterized by Raman, XRD, UV–Vis, SEM and CH instrument revealing that the hybrid nanostructure was composed of few-layered MoS_2 nanosheets with enlarged interlayer distance, suitable for electron transfer process. PANi-α-Fe_2O_3–MoS_2-DNA hybrid nanostructure significantly exhibited better electro catalytic activity toward simultaneous detection of pollutants such as hydroquinone (HQ), catechol (CC), resorcinol (RS) and nitrite (NO_2^-). The hybrid electro catalyst shows simultaneous linear response of HQ, CC, RS and NO_2^- in the concentration range of 500 nM–300 μM, 400 nM–300 μM, 200 nM-300 μM and 300 nM-300 μM with lowest detection limits 180, 178, 95 and 102 nM respectively. In addition, the biosensor exhibited excellent sensitivity, selectivity and stability. The real time application of PANi-α-Fe_2O_3–MoS_2-DNA hybrid nanostructure demonstrated with satisfactory results in detecting HQ, CC, RS and NO_2^- in well water and pond water samples.

1. Introduction

Monitoring of phenolic compounds such as Catechol (CC), Resorcinol (RS), and Hydroquinone (HQ) in the food industry and environment has focused a great concern recently since their antioxidant behavior being helpful to control cardiovascular and cancer diseases (Huang et al., 2015; Zahedi et al., 2017). Moreover, some phenols are ubiquitous pollutants that spoil the natural water through the effluents of chemical industrial performance which turn into toxic in animals and plants, because they easily penetrate the skin and cell membranes. Even at small concentrations (<1 ppm), phenolic compounds affect the taste and odor of drinking water and sea water (Lv et al., 2010). The toxic pollutants in waste water usually interact with DNA, leading to the damage to human health, so, it is highly needed to design an environmental sensor for rapid screening of these pollutants (Umare et al., 2018). The absorption of CC or HQ from the gastrointestinal tract can induce some serious diseases such as renal tube deterioration and liver function decrease (Ansari et al., 2008). In addition, lungful of air in high concentration of RS can directly lead to the death of human beings (Becerra-Herrera et al., 2014). Similarly, Nitrite (NO_2^-) is one of the major inorganic pollutants found in food, environment, industry and physiological systems. A constant consumption of these ions can develop serious complications on human health and aquatic environment (Li et al., 2014). So, concerns over the effects of (NO_2^-) exposure have led to the significant contributions in analytical chemistry. Normally, these pollutants coexist as in ecological samples. Due to their low degradability and high toxicity in the natural environment, it is essential to design a rapid and simple analytical technique for their detection. To date, numerous analytical routes have been developed to accurately determine the pollutants such as liquid chromatography high-performance (Lu et al., 2014) chemiluminescence (Nagaraja et al., 2001) fluorescence (Liao et al., 2012) mass spectrometry (He et al., 2012) capillary electrochromatography (Medina-Plaza et al., 2015) spectrophotometry (Ahammad et al., 2011) and electrochemical techniques (Liu et al., 2010; Munir et al., 2017). Among them, electrochemical route focuses significant consideration owing to their advantages of low cost, fast response, high selectivity and excellent sensitivity. Since the pollutants have analogous stereochemical structure and close redox potentials, the simultaneous detection of them is a challenging task. In order to flawlessly detect, some functional materials such as metal sulphides (Ji et al., 2016) carbon based materials (Pramanik et al., 2018) quantum dots (Lee et al., 2002) have been employed as the sensing platform for simultaneous determination of the environmental pollutants. However, these samples undergo high toxicity, complicated synthesis process, poor

* Corresponding author.
E-mail address: wilson.j2008@yahoo.com (R.R.J. Wilson).

https://doi.org/10.1016/j.bcab.2019.101352
Received 26 March 2019; Received in revised form 4 September 2019; Accepted 18 September 2019
Available online 18 September 2019

analytical performance and laborious. Therefore, it is still a challenge to demonstrate convenient and robust sensing material for the simultaneous detection of these pollutants.

Generally, polyaniline (PANi) is one of the smart conducting polymers attracted major attention for their applications in a variety of fields microelectronic devices, light weight batteries, sensors, super capacitors, microwave absorption inhibition, chemical and biological sensors, actuators and microelectronic devices due to its exclusive electrical, electrochemical properties, easy polymerization, high environmental stability and low cost of monomer (Matte et al., 2010).

For analogous reasons, high concern on nanostructured metal oxides are focused owing to their enhanced electron-transfer kinetics, strong adsorption, microenvironments for the immobilization of biomolecules and improved electrochemical characteristics ((Miao et al., 2017). Maiyalagan et al., 2013 reported that α-Fe_2O_3 demonstrated the noble metallic behavior and also observed possessing an intrinsic enzyme-mimicking activity as that of natural horseradish peroxidase. Hence, α-Fe_2O_3 could be utilized for enzyme free biosensor applications. Very recently, our group demonstrated the behavior of α-Fe_2O_3 key role in giving the maximum detection limit due to its catalytic and enhanced conductive behavior on combination with Au–Pd bimetal (Sumathi. et al., 2017) and the interaction of DNA with Fe_2O_3 based composite has also been studied (Sumathi et al., 2015).

Molybdenum disulfide (MoS_2) composed of S–Mo–S triple layers a newly discovered band gap-adjustable semiconductor, having sandwich structure similar to graphene (Bhandari et al., 2013) and catalytic activity originates from the sulfur edges of MoS_2 layers while inner planes are catalytically inert which is highly applicable in the fields of electrochemistry, capacitors, catalysts, sensors and lithium-ion batteries (Mittal et al., 2015; Yan et al., 2017).

Very recently, biomolecules like amino acids, nucleic acids, proteins, and peptides have attracted the researchers to use them as templates for the fabrication of nanostructured materials (Mirkin et al., 2000; Berti et al., 2005). Among the various biomolecules, deoxyribonucleic acid (DNA) has been a smart material to design inorganic nanostructures due to simplicity, experimental design, well-characterized, controllable and easily compatible behavior. The sugar molecules and phosphate groups of DNA can combine with different metal/polymer cations through electrostatic interactions which in turn enhance electron transfer process significantly (Keren et al., 2013; Jiménez-Monroy et al., 2017). Obviously, the electrochemical route could provide highly sensitive and selective simultaneous determination of these pollutants. Up to now, no literature is simultaneously sensing the four pollutants.

The study/analysis of interaction of phosphate and sugar groups in DNA in the hybrid nanostructure with hydroxyl groups of environmental pollutants is the novelty of our work. This work is to understand the mixed electronic/ionic transport in conducting polymer-metal oxide-dichalcogenide-biomolecule hybrid nanostructure to construct a novel device with improved catalytic activity of pollutant samples. MoS_2 affords more spacing for insertion of other materials in the composite (Seidel et al., 2004). Interestingly, the role of DNA is analyzed in terms of reduction potential in environmental pollutants sensing and its detection range. The corresponding schematic sensing mechanism is revealed in Scheme 1.

2. Experimental procedure

2.1. Reagents and materials

Aniline, sodium molybdate ($Na_2MoO_4{\cdot}2H_2O$), ammonium persulfate (APS), HQ, CC, RS, NO_2^- and ethanol were purchased from Sigma-Aldrich Co. Ltd (India). $FeCl_3$, glucose, sodium hydroxide pellet and thiourea were obtained from Sisco research laboratories, Mumbai. Double-stranded herring testes DNA with an average molecular weight 50 kbps (base pairs), ds-DNA is simply denoted as DNA throughout this paper. The 15mer synthetic oligonucleotide was procured from MWG biotech, Ebersberg, Germany with HPLC purification. Their DNA base sequences are given below:

- Double strand DNA: 5′-TAT CTA CGT ACA TGT-3′

The stock DNA solution (0.06 g per 50 mL) was prepared by mixing a measured amount of deionized (DI) water. All aqueous solutions were prepared by DI water.

2.2. Instruments and measurements

The surface morphology of the prepared materials was performed by SEM with EDAX (Quanta FEG 250) from FEI (S.E.A) PTE LTC of USA; X-ray diffraction (XRD) was investigated using Powder X-Ray Diffractometer D8 with CuKα advanced radiation (1.5418 Å) in the range if 20–80 diameter. The Raman spectrum was noted using an imaging

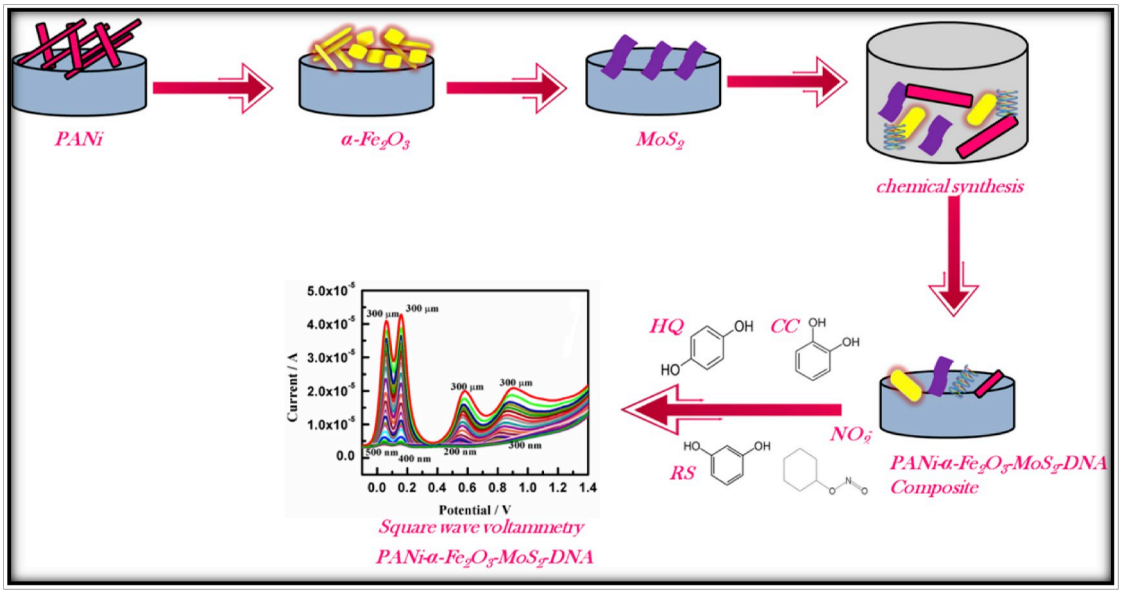

Scheme 1. Illustration of preparation of PANi-α-Fe_2O_3–MoS_2-DNA hybrid nanostructure and HQ, CC, RS and NO_2^- detection.

spectrograph (model STR 500 mm focal length) Micro-Laser Raman Seiki in Japan. UV studies were carried out using an evolution 201 UV–Visible spectrophotometer. The CHI 6005D electro-chemical workstation from Austin in USA was utilized with a GC working electrode (0.07 cm^{-2}), an Ag/AgCl (3.0M KCl) reference electrode and a platinum wire auxiliary electrode to perform the electrochemical studies. All the measurements were executed in PBS (phosphate buffer solution) under nitrogen atmosphere.

2.3. Polyaniline nanotubes synthesis

100 μL of aniline with 200 mg of APS was dissolved in DI water in a volumetric flask 50 mL of solution and allowed to stirring for 30 min. After that, dark greenish color obtained was deep freezed for 36 h, filtered and dried out.

2.4. α-Fe_2O_3 nanorods synthesis

Ferric chloride 1.0 g was taken and then sodium hydroxide pellet (NaOH) 0.2 g mixed in a beaker of 100 mL DI water. This solution was then stirred and heated using autoclave to160 °C for 18 h, lastly the product was centrifuged, washed and dried.

2.5. DNA stock solution preparation

In a typical synthesis, 10 mL of stock DNA solution (0.06 g per 50 mL) was synthesized by mixing a measured amount of DI water. The DNA solution was stirred overnight to get homogeneous DNA solution without any pop-up of adenine and guanine bases in DNA.

2.6. PANi-α-Fe_2O_3–MoS_2-DNA hybrid nanostructure

100 μL of aniline with 200 mg of APS was dissolved in DI water in a

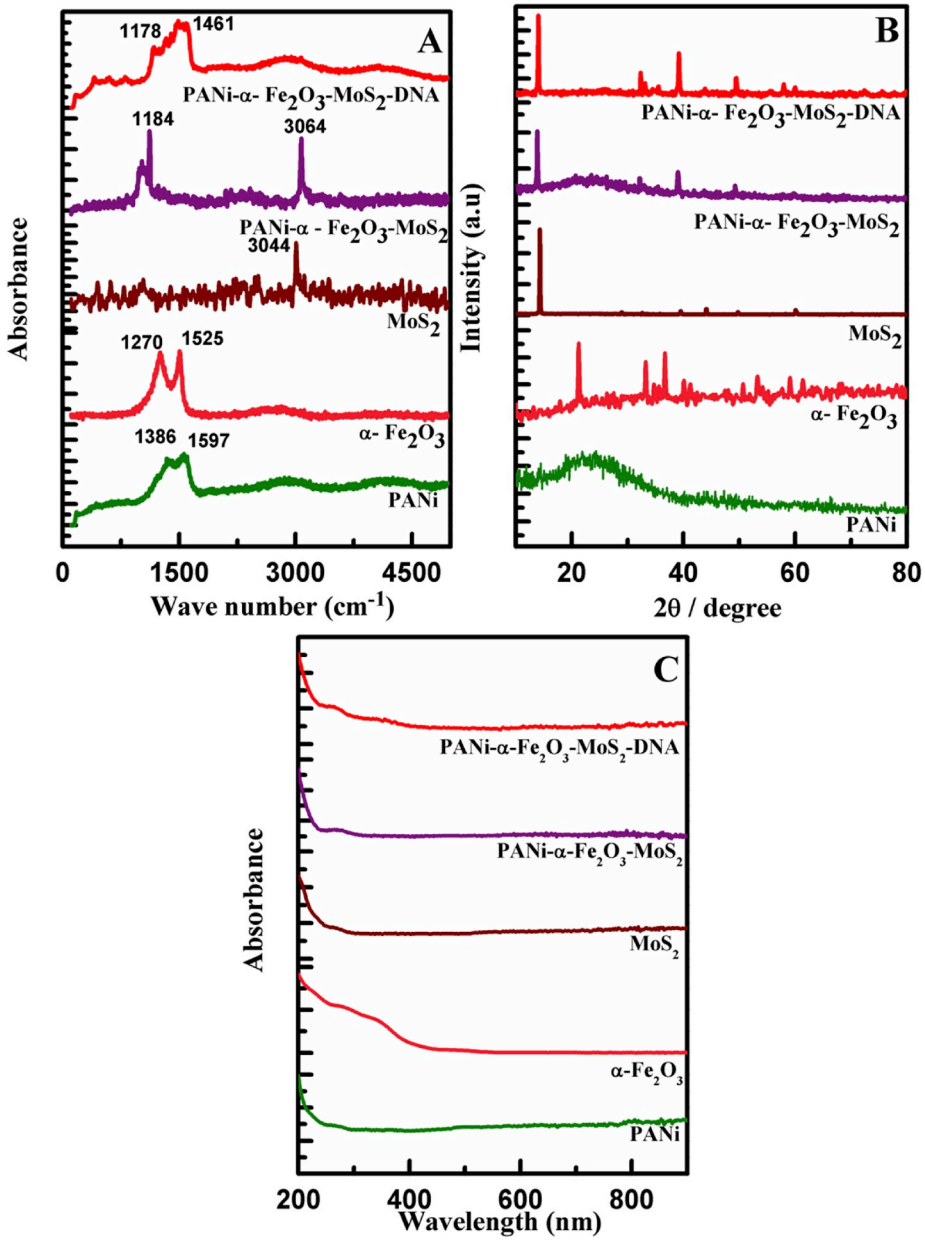

Fig. 1. (A) Raman spectra (B) XRD patterns (C) UV patterns of PANi, α-Fe_2O_3, MoS_2, PANi-α-Fe_2O_3–MoS_2 composite and PANi-α-Fe_2O_3–MoS_2-DNA hybrid nanostructure.

volumetric flask 50 mL of solution and allowed to stirring for 30 min. Then, MoS_2 (0.005 g), α-Fe_2O_3 (0.005 g) and DNA (2 mL) stock solution were also added. After 30 min final solution was kept on deep freezing for 36 h, then filtered and dried out.

3. Results and discussion

3.1. Structural analysis

3.1.1. Raman study

Raman spectra displays (Fig. 1A) the conventional peaks indexed at 1184 and 1516 cm^{-1}, which corresponds to C═C stretching vibration of quinoid ring, C–H bending of the quinoid ring of PANi (Wang et al., 2015), while peak at 3044 cm^{-1} confirms the rod-shaped α-Fe_2O_3 single-crystalline nature. The two broad peaks show at 1270 cm^{-1} (D-band) and 1525 cm^{-1} (G-band), with some additional peaks of hexagonal structured MoS_2 presence (Yan et al., 2010). Further, it is confirmed from the PANi-α-Fe_2O_3–MoS_2 composite spectra that the strong peaks of G and D band of MoS_2 found unchanged indicating no structural change in the composite and further new peaks appeared support the composite formation (Sevilla et al., 2014). In the PANi-α-Fe_2O_3–MoS_2 composite, low intensity peaks of PANi at 1516 cm^{-1} with C═C stretching vibration, α-Fe_2O_3 at 3044 cm^{-1} of O–H stretching vibration, the two broad peaks at 1270 cm^{-1} and 1525 cm^{-1} represent the C═C stretching vibration, with some additional peaks of hexagonal of structured MoS_2 presence are very well witnessed. Moreover, the peak of DNA presence at 1461 cm^{-1} due to C–N stretching vibration confirms the PANi-α-Fe_2O_3–MoS_2-DNA hybrid nanostructure formation (Lim et al., 2010). It can be concluded that the changes in peak intensity and new peak formation and morphological rearrangements have been well confirmed the hybrid structure formation.

3.1.2. XRD study

X-ray diffraction (XRD) analysis is used to investigate the crystallinity of as prepared materials (Fig. 1B). The broad centered around 25° is ascribed to the periodicity parallel and perpendicular to the polymer chain with small crystallinity of PANi (Soon et al., 2011). In Fig. 1B shows the α-Fe_2O_3 characteristic peaks at 33.23°, 36.56°, 50.83°, 53.25°, 61.41° with high purity and crystallinity (JCPDS card no.33–0664). The rods of α-Fe_2O_3, which has the rhombohedral structure well matched for iron oxide and no other hydroxide, maghemite, magnetite peaks are observed in the hematite phase (Chang et al., 2015). The sharp diffraction peak at 14.17° and weak emerging peaks at 44.14° and 60.20°, confirm the presence of MoS_2 with hexagonal structure (Zhou et al., 2012). As shown in the PANi-α-Fe_2O_3–MoS_2 sample, the observed diminished intensity/peak shift due to the interaction and composite formation. It is also reported a strong interaction between amine group of PANi and MoS_2 is probably due to the hydrogen bonding which is significantly enrich the electric conductivity. Similarly, the presence of ferrite particles in the composite formation is also confirmed (Sumathi et al., 2016). The pattern of PANi-α-Fe_2O_3–MoS_2-DNA hybrid revealed the increased peak intensity with different diffraction angle of 2θ value at 14°, 26°, 32°,33° 35°, 39° suggesting the existence of DNA with well crystallinity which is attributed to strong adsorption of crystalline adhesive interfaces. Thus, the XRD results suggested that PANi-α-Fe_2O_3–MoS_2-DNA hybrid with improved crystalline behavior highly desirable for biosensing applications (Liang et al., 2013).

3.1.3. UV study

Fig. 1C shows the absorption spectra of PANi at 630 nm, assigned to π-π* transition (Kundu et al., 2013). The optical absorption property of inter-band transition of hematite taking place at approximately above 360 nm tells the α-Fe_2O_3 presence (Yang et al., 2010). MoS_2 obviously gives the carbon's presence with sharp peak at 220 nm (Nimbalkar et al., 2016). In UV absorption spectrum of PANi-α-Fe_2O_3–MoS_2 nanocomposite, π–π* transition of PANi is shifted to 260 nm due to the interaction between the α-Fe_2O_3 and quinoid ring of PANi. The UV absorption spectrum of PANi-α-Fe_2O_3–MoS_2-DNA hybrid nanostructure film formation results of strong π−π stacking interaction between PANi and DNA. The band gap energies were calculated as 3.37 eV, 3.02 eV for PANi and PANi-α-Fe_2O_3–MoS_2-DNA composite respectively, by plotting Tauc's graphs between α (hυ) $^{1/2}$ versus photon energy (hυ) (Fig.S2). The low band gap of PANi-α-Fe_2O_3–MoS_2-DNA value is responsible for better catalytic activity for the detection of pollutants.

3.2. Morphology analysis

The SEM image of PANi nanotube in Fig. 2A is quite in uniform size ~140 nm. Fig. 2B shows the MoS_2 nanosheets with slightly folded dentations on the edges, which considerably enhance the exposure of active edge sites (Rahmat et al., 2017). While, Fig. 2C reveals the well dispersed regular and attractive rod shapes of Fe_2O_3 with crystalline morphology, and average particle size ~96 nm. The presence of α-Fe_2O_3 and PANi found embedded over the MoS_2 sheets is clearly seen in Fig. 2D. The DNA wrapped on the α-Fe_2O_3-PANi-MoS_2 composite is exhibited in Fig. 2E. The EDAX measurement also reports their presence in the hybrid nanostructure (Fig. 2F).

3.3. CV & EIS studies on PANi-α-Fe_2O_3 – MoS_2-DNA modified GCE

3.3.1. Cyclic voltammetry

The CVs of the different modified electrodes recorded in the presence of 1 mM $[Fe(CN)_6]^{3-/4-}$ in 0.1 M KCl at a scan rate 50 mV s^{-1} are shown in Fig. 3A. As seen in Fig. 3A, at the bare GCE, a pair of well defined redox peak is observed with peak to peak separation value 70 mV. But, up and downs of current values observed for the MoS_2 (curve b), α-Fe_2O_3 (curve c), PANi (curve d) and PANi-α-Fe_2O_3–MoS_2 composite (curve e). Interestingly, the PANi-α-Fe_2O_3–MoS_2-DNA hybrid nanostructure modified electrode showed maximum value of current compared other modified GCE signature its excellent electrochemical performances. This is attributed to electrostatic interaction of DNA with other materials in the hybrid and supported with literature (Prusty et al., 2017). These result shows good agreement with the charge transfer resistance values obtained from EIS measurements.

3.3.2. Electrochemical impedance spectroscopy

It is well known that EIS is a powerful tool for studying the surface properties of modified electrodes. The charge transport process of modified GCE was studied by monitoring charge transfer resistance (R_{CT}) at the electrode – electrolyte interface (Fig. 3B). The value of the charge transfer resistance (R_{CT}) for the bare GCE, PANi, α-Fe_2O_3, MoS_2, PANi-α-Fe_2O_3–MoS_2 composite and PANi-α-Fe_2O_3–MoS_2-DNA hybrid nanostructure modified GCEs were estimated to be 281, 173, 150, 371, 90 and 23 Ωcm^{-2} respectively. From the R_{CT} value of PANi-α-Fe_2O_3–MoS_2-DNA modified GCE, it is understood that high electron transfer ability of the system and supports with CV studies.

3.4. Electrocatalytic oxidation of HQ, CC, RS and NO_2^-

The CV was performed in the potential range of −0.1–1.5V in presence 0.1M PBS with pH 7 (Fig. 4A). Then, 100 μM each HQ, CC, RS and NO_2^- at 50 mVs^{-1} was injected into the PBS. Then the GC electrode was modified with (a) bare (b PANi (c) α-Fe_2O_3 (d) MoS_2 (e) PANi-α-Fe_2O_3–MoS_2 composite (f) PANi-α-Fe_2O_3–MoS_2-DNA hybrid nanostructure samples by drop casting technique separately and allowed to dry for 1hr and then put into the electrochemical cell to study their current values. With the PANi modified GCE, an increase in cathodic peak currents are 11, 15, 16 and 17 μA. The attachment of α-Fe_2O_3 results 5.7, 8.2, 9.4 and 11 μA, while on MoS_2 modified electrode shows 4.9, 8.5, 10 and 11 μA. In the same way, PANi-α-Fe_2O_3–MoS_2 composite modified electrode exhibited the current value to 10, 13, 16 and 29 μA. Interestingly, PANi-α-Fe_2O_3–MoS_2-DNA hybrid nanostructure modified

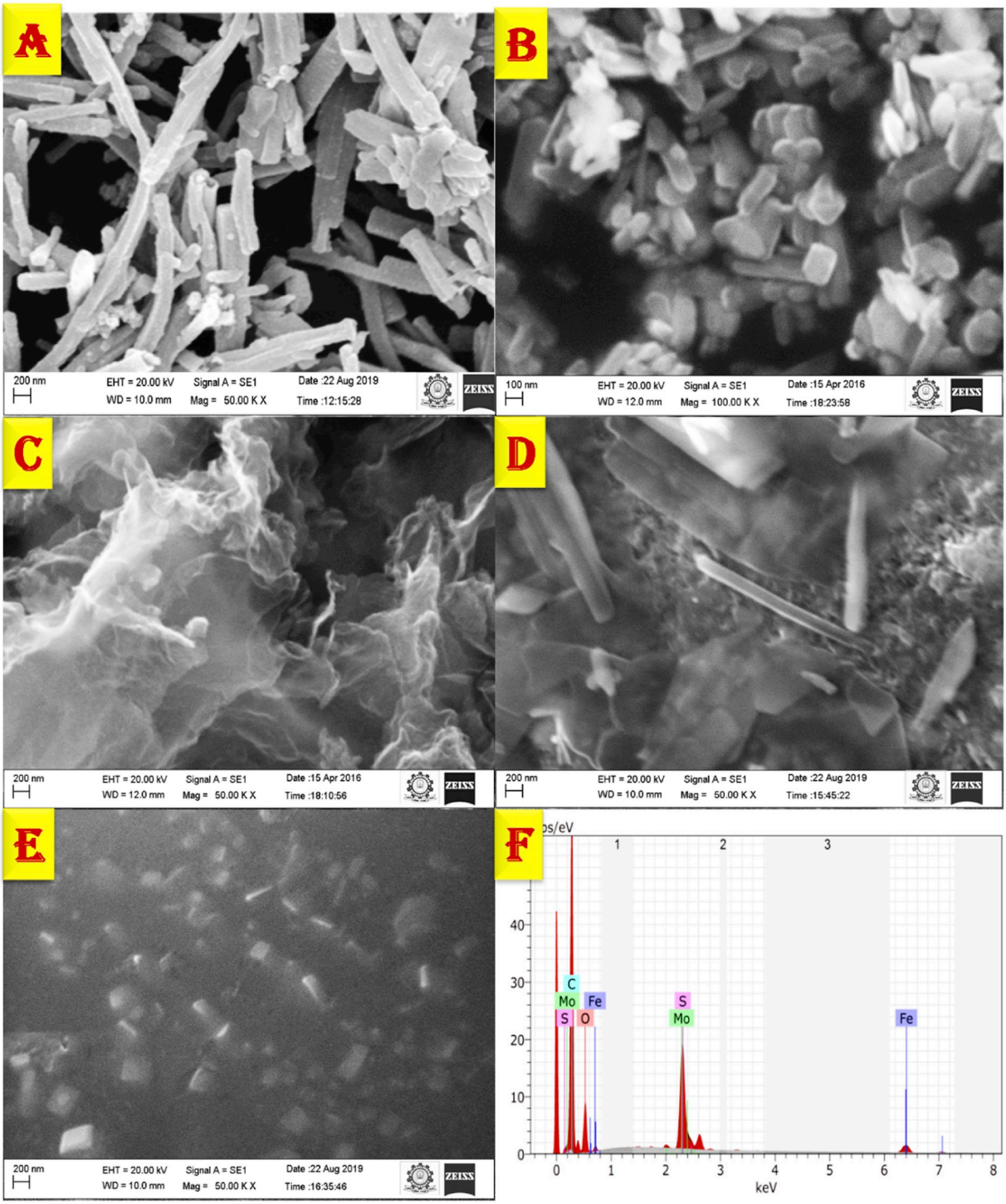

Fig. 2. SEM images of (A) PANi nanotubes (B) α-Fe_2O_3 nanorods (C) MoS_2 nanosheets (D) PANi-α-Fe_2O_3–MoS_2 composite (E) PANi-α-Fe_2O_3–MoS_2-DNA hybrid nanostructure (F) EDAX spectrum of hybrid nanostructure.

electrode depicts the maximum current of 15, 16, 30 and 49 μA owing to electrostatic interaction between the sample and analytes.

Since electrons/protons participate in the redox chemistry of biomolecules, the redox peak current and potential are pH dependent. As shown in Fig. 4B, the PANi- MoS_2-α-Fe_2O_3- DNA hybrid nanostructure system generated the maximum catalytic current at pH 7 and gradually decreased its catalytic activity when the pH was changed to neutral and basic values.

On comparing the slopes observed in inset Fig. 5B, PANi-α-Fe_2O_3–MoS_2-DNA hybrid found steeper slope comparatively with PANi-α-Fe_2O_3–MoS_2 composite (Fig. 5A), further verifying the catalytic role in the electrochemical oxidation of HQ, CC, RS and NO_2^- analytes (Li et al., 2017).

3.5. Individual electrocatalytic oxidation of HQ, CC, RS and NO_2^-

The SWV of different modified electrodes oxidation peak potentials of HQ, CC, RS and NO_2^- are investigated (Fig. 6). The linear responses for the individual determination of HQ, CC, RS and NO_2^- were observed in the concentration ranges of 900 nM -1mM, 700 nM–1mM, 300 nM-30

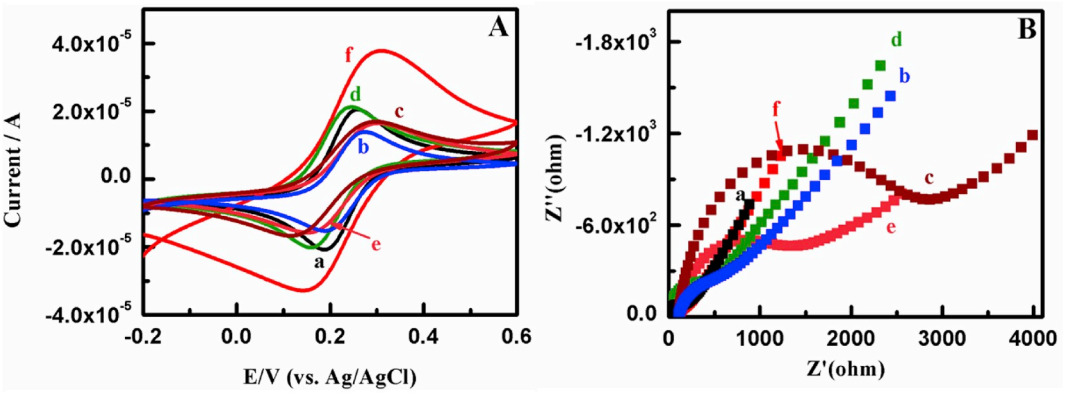

Fig. 3. (A) CV & (B) EIS Profiles of the modified GC electrodes in presence of 1 mM $[Fe(CN)_6]^{3-/4-}$ in 0.1 M KCl at a scan rate of 50 mV s^{-1}. Curves: (a) bare GC, (b) PANi, (c) α-Fe_2O_3, (d) MoS_2, (e) PANi-α-Fe_2O_3–MoS_2 composite, (f) PANi-α-Fe_2O_3–MoS_2-DNA hybrid nanostructure modified GC electrodes.

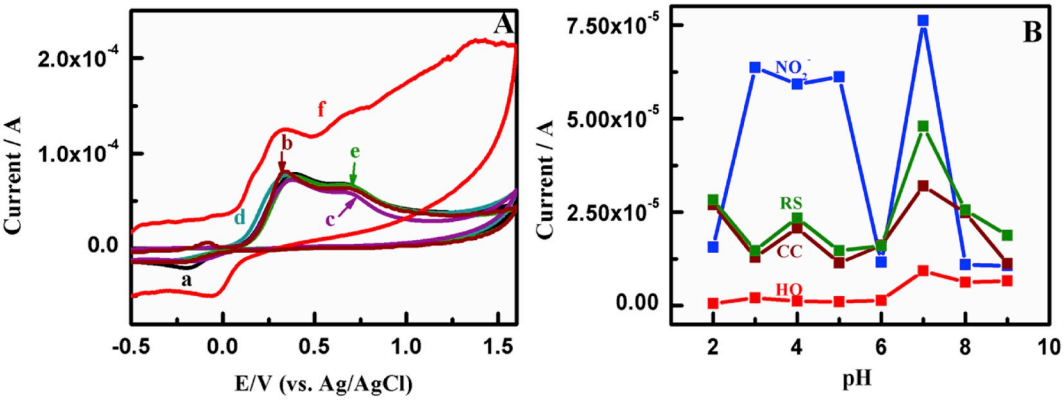

Fig. 4. CVs: (A) (a) bare (b) PANi (c) α-Fe_2O_3 (d) MoS_2 (e) PANi-α-Fe_2O_3–MoS_2 composite (f) PANi-α-Fe_2O_3–MoS_2-DNA hybrid nanostructure in 100 μM HQ, CC, RS and NO^{2-} at 50 mV s^{-1} (B) pH versus current.

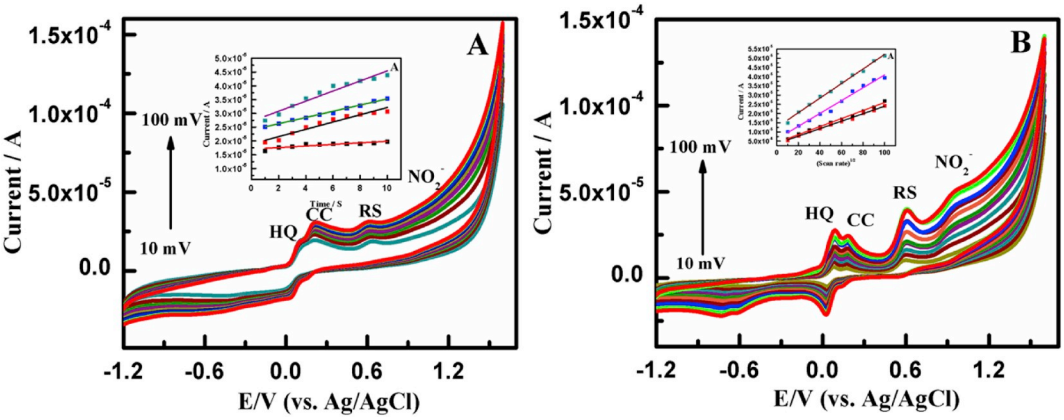

Fig. 5. CVs obtained for HQ, CC, RS and NO_2^- of 100 μM (A) PANi-α-Fe_2O_3–MoS_2 composite (B) PANi-α-Fe_2O_3–MoS_2-DNA hybrid nanostructure modified electrode recorded in PBS (pH 7.0) at different scan rates 10–100 mV s^{-1}.

μM and 700 nM -1mM with detection limits of 296, 90,110 and 108 nM using PANi-α-Fe_2O_3–MoS_2 composite (Fig. S3). Interestingly, PANi-α-Fe_2O_3–MoS_2-DNA hybrid nanostructure exhibited significant wider concentration ranges of 400 nM -1mM, 200 nM–1mM, 100 nM-700 μM and 100 nM-1mM with detection limit of 93, 40, 38 and 94 nM of HQ, CC, RS and NO_2^- respectively. On comparing the PANi-α-Fe_2O_3–MoS_2 composite with PANi-α-Fe_2O_3–MoS_2-DNA hybrid nanostructure, it was observed that DNA could play a key role provided the maximum detection limit due to its catalytic and enhanced conductive behavior upon combination with composite (Ali et al., 2012).

As shown in Fig. 7, the peaks were obtained by changing the concentration of one analyte while keeping the concentrations of the others as constant. The experimental results confirm that no obvious interferences were observed for the determination of one analyte in the presence of other three analytes kept constant.

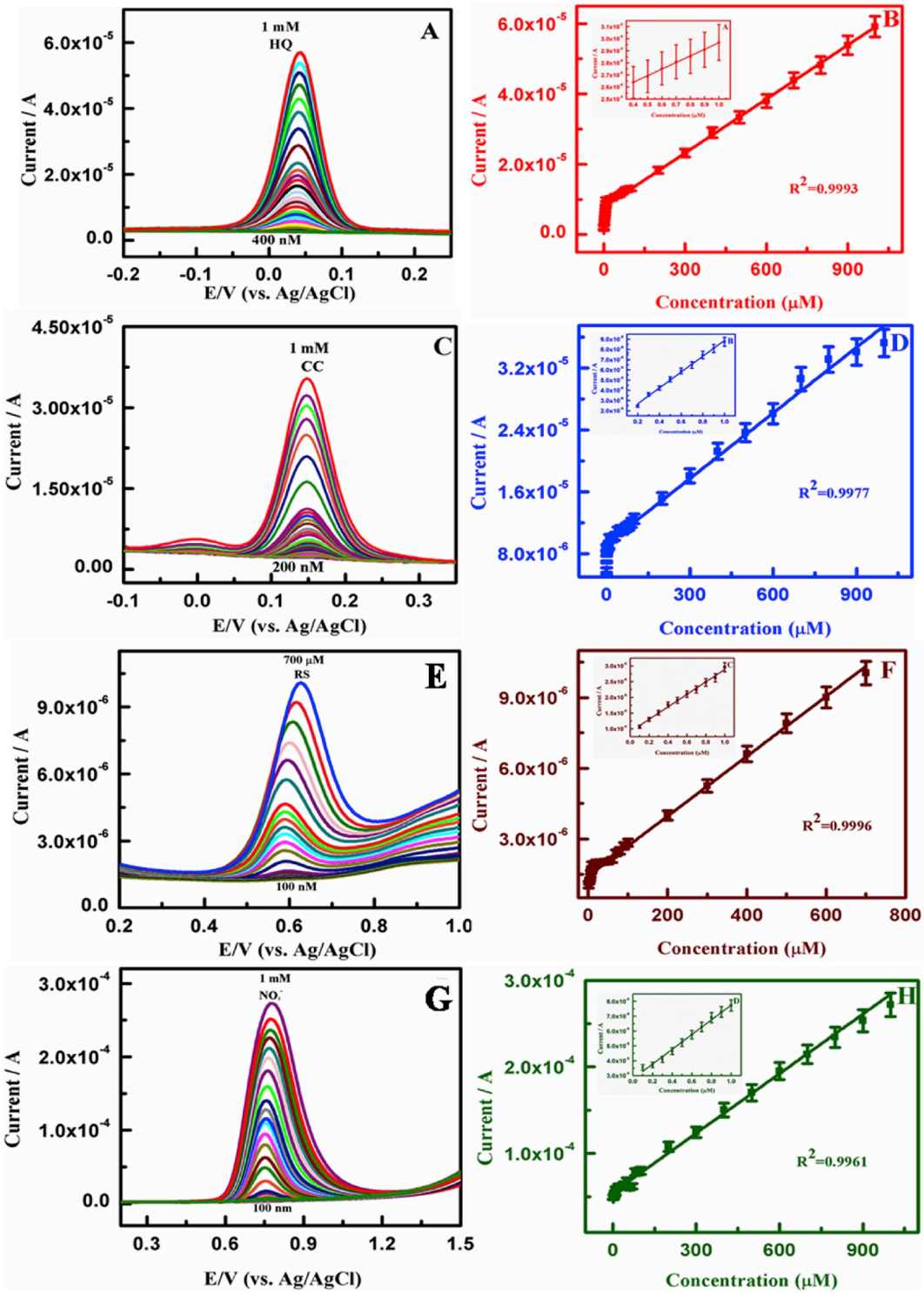

Fig. 6. SWV profiles (A) 400 nM–1 mM HQ (C) 200 nM-1mM CC(E) 100 nM-700 μM RS (G) 100 nM–1 mM NO_2^- (B) (D) (F) (H) plot of the oxidation peak current against concentration of HQ,CC, RS and NO_2^- at PANi-α-Fe_2O_3–MoS_2-DNA hybrid nanostructure GCE in 0.1 M PBS (pH 7.0).

3.6. Simultaneous catalytic oxidation of HQ, CC, RS and NO_2^- at PANi-α-Fe_2O_3–MoS_2 and PANi-α-Fe_2O_3–MoS_2-DNA modified electrode

In the simultaneous determination of PANi-α-Fe_2O_3–MoS_2 composite, the linear responses of HQ, CC, RS and NO_2^- were obtained in the concentration ranges of 3 μM–900 μM, 1 μM–900 μM, 1 μM–900 μM and 2 μM–900 μM with lower detection limits 2.1 μM, 4.4 μM, 2.09 μM and 1.93 μM (Fig. S4). Remarkably, the PANi-α-Fe_2O_3–MoS_2-DNA hybrid exhibited the concentration range of 500 nM-300 μM, 400 nM-300 μM, 200 nM-300 μM and 300 nM-300 μM with lower detection limits 180, 178, 95 and 102 nM (Fig. 8). Three important points have been observed: (i) the DNA coated hybrid nanostructure significantly provides lower detection range of HQ, CC, RS and NO_2^- respectively compared to the PANi-α-Fe_2O_3–MoS_2 composite (ii) reduced the oxidation potential of analytes by 10, 9, 24 and 81 mV compared to former electrode (iii) no reports are found to be the best of our

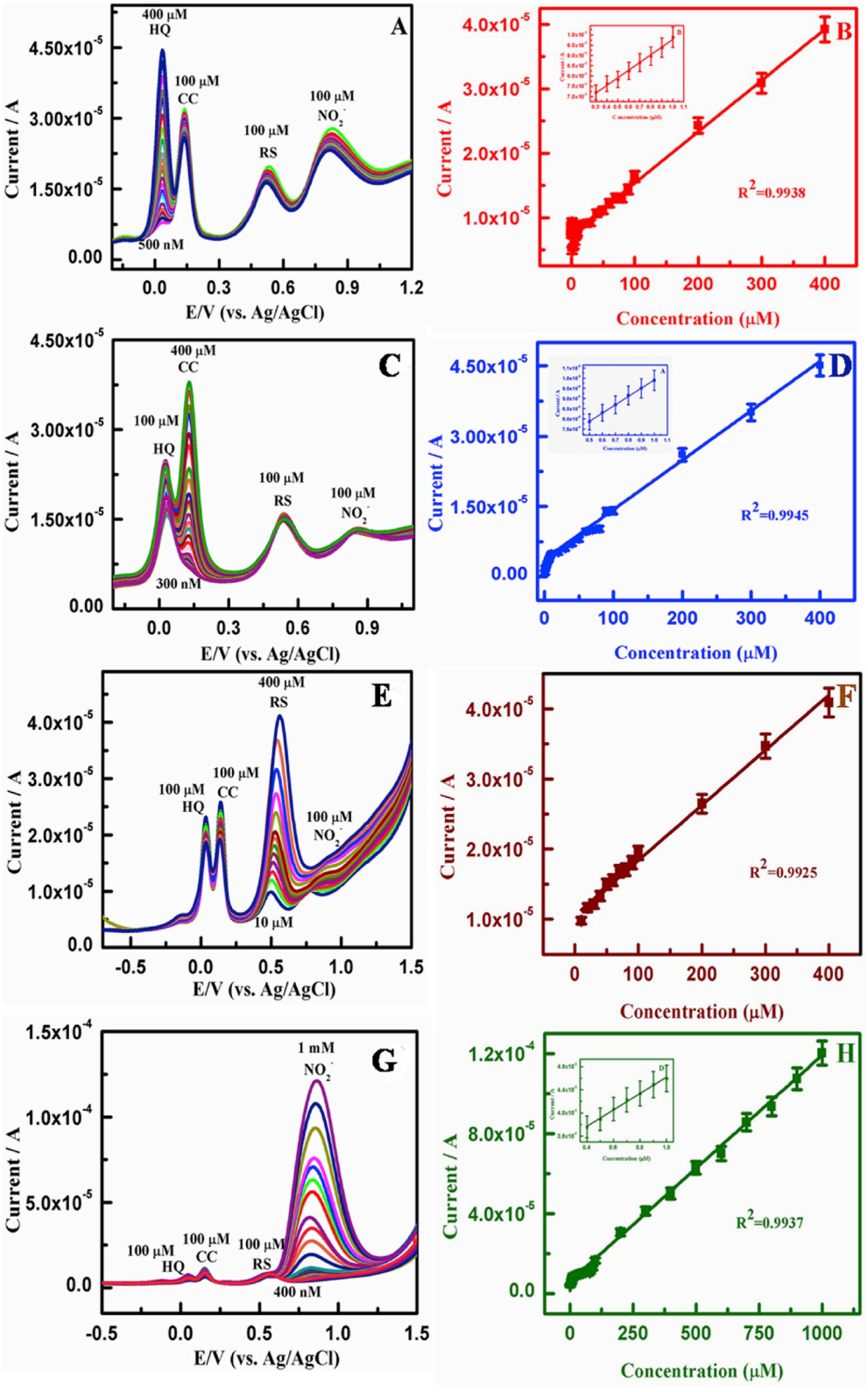

Fig. 7. SWVs obtained for various concentrations (A) HQ (500 nM-1mM) (B) CC (300 nM −1 mM) (C) RS (10 µM–700 µM) (D) NO_2^- (400 nM-1mM) in presence of 100 µM each analytes at PANi-α-Fe_2O_3–MoS_2-DNA modified GCE in 0.1 M PBS (pH 7.0).

knowledge which exhibits the simultaneous detection of these 4 analytes. A strong interaction and fast formation of PANi and DNA in the hybrid due to electrostatic attraction between phosphate groups of the DNA and PANi claim the enhanced electrocatalytic activity. Moreover, it is believed that in the PANi -DNA system increased the conductivity due to modulation ability of DNA conformation in the redox process also supported for the enhanced catalytic behavior. Hence, the design of this scaffold with DNA could be used for the fabrication of nanostructures catalyst for biosensing applications (Vyborna et al., 2017). The electrostatic, covalent bonding and π-π interaction are the prime factors

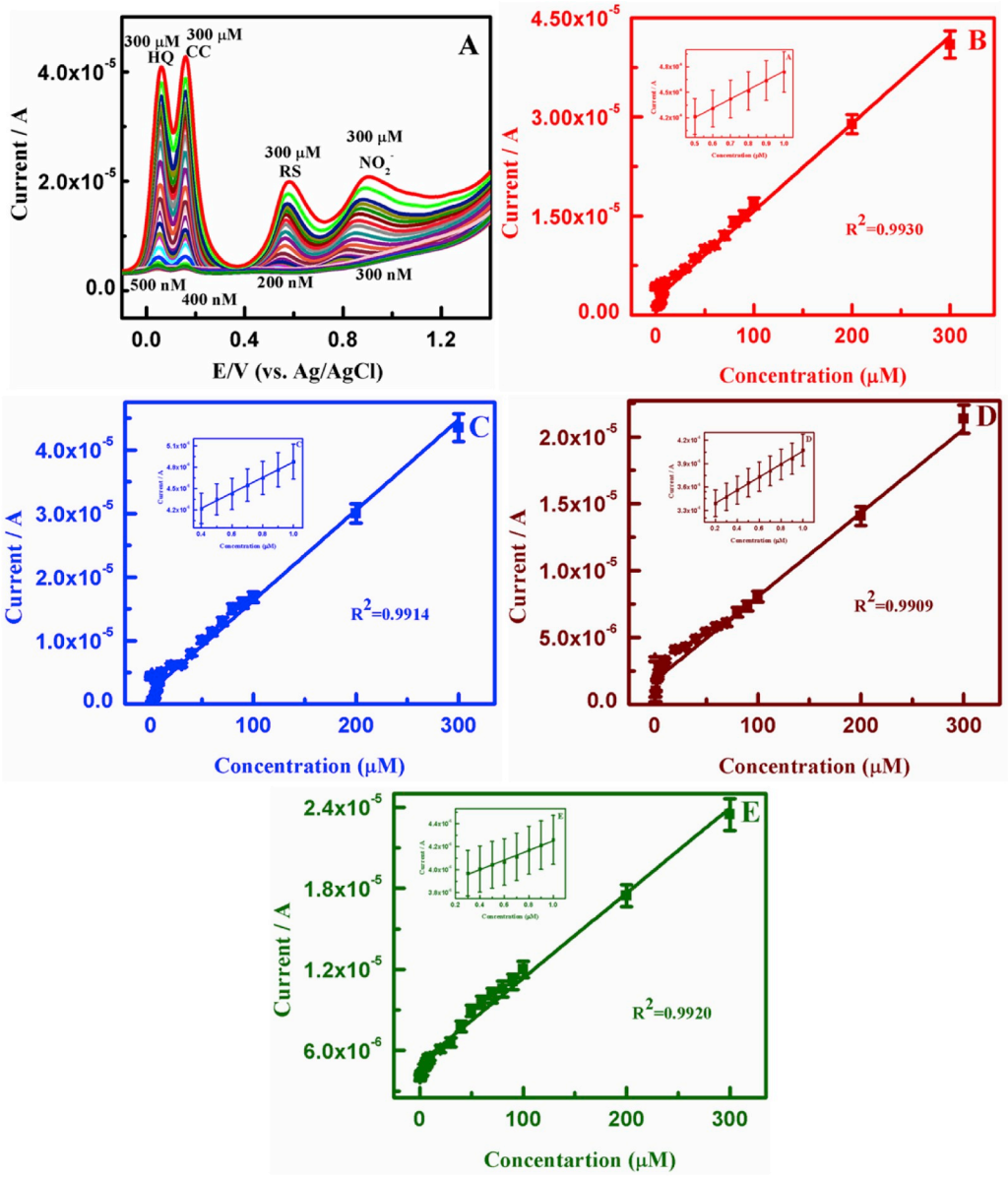

Fig. 8. (A) SWVs obtained for various concentrations of HQ (500 nM–300 µM), CC (400 nM–300 µM), RS (200 nM-300 µM) and NO_2 (300 nM-300 µM) at PANi-α-Fe_2O_3–MoS_2-DNA hybrid nanostructure in 0.1M PBS (pH 7.0) and (B),(C),(D) & (E) are plots of the oxidation peak currents as a function of various concentrations of HQ, CC, RS and NO_2^-.

between conjugated interface and DNA bases for the pollutants sensing. Amine group of PANi can be easily attracted with –OH group of environment polluntants. Similarly, the phosphate and sugar groups in DNA exhibited efficient electrostatic interaction with the pollutants. The corresponding detection limits and response ranges of the different modified electrodes are listed (Table S3) for comparison.

3.7. Reproducibility and stability

The reproducibility of the PANi-α-Fe_2O_3–MoS_2-DNA hybrid nanostructure was investigated by SWV responses of HQ, CC, RS and NO_2^-. The relative standard deviation (R.S.D) responses for six independent electrodes were 5.6%. The stability of the fabricated sensor with PANi-α-Fe_2O_3–MoS_2 composite and PANi-α-Fe_2O_3–MoS_2-DNA hybrid nanostructure was subjected to continuous 100 cycles in presence of each 500 µM of analytes (Fig. S5). The long-term stability of the electrode stored at 4 °C was measured after one month of storage in dry conditions. The electrode retained 86% of its initial response. These results demonstrate that the modified electrodes possessed satisfactory reproducibility and tremendous stability for analytical applications.

3.8. Practical applications

The anti-interference ability of the PANi-α-Fe_2O_3–MoS_2-DNA hybrid nanostructure was examined by the addition of several types of ions and other small molecules to PBS solution containing 100 µM HQ, CC, RS and NO_2^-. (Fig. S6 and Table S1). In this study, different potentials such as HQ 0.1V, CC 0.3V, RS 0.6V and NO_2^- 0.8V were applied. No significant interference was observed in the presence 10 fold excess of ascorbic acid, KCl, riboflavin, folic acid, $MgCl_3$, uric acid and glucose. It is clear that the proposed sensor exhibited good selectivity for the determination of HQ, CC, RS and NO_2^-. The utilization of the PANi-α-Fe_2O_3–MoS_2-DNA hybrid nanostructure sensor in real samples was also studied by standard addition method in well water and tap water samples.

The well-water and tap water were diluted 10 times with 0.1 M PBS solution (pH 7.0) without any other treatment before measurement.

While adding the diluted sample, a sharp peak appeared for HQ, CC, RS and NO_2^- at 0.02 V, 0.14 V, 0.51 V and 0.88 V for 10 μM concentration of well water and 0.03 V, 0.14 V, 0.55 V and 0.85 V for 10 μM concentration of tap water. For different concentration (10–90 μM) of well-water sample and (1–100 μM) of tap water sample, the corresponding HQ, CC, RS and NO_2^- peaks were recorded in Fig. S7. All the details of real sample analysis results are summarized in Table S2.

4. Conclusion

The fabricated PANi-α-Fe_2O_3–MoS_2-DNA hybrid nanostructure modified electrodes, which integrated the unique behavior provide superior currents (α-Fe_2O_3- enzymatic activity, MoS_2 mimics activity of graphene and DNA-catalytic activity) better electrochemical performance for the oxidation of HQ, CC, RS and NO_2^- compared to the PANi-α-Fe_2O_3–MoS_2/GCE electrode possibly due to the high surface area and synergistic effect of the composite material with DNA. It is demonstrated that DNA based hybrid significantly exhibits wider detection range, more sensitivity and high electro catalytic activity. Additionally, the DNA modified hybrid structure pave the platform for high degree of potential application in biomedical and non-corrosive device fabrications.

Conflicts of interest

The authors declare no conflict of interest.

Acknowledgement

The author J.W. gratefully acknowledges the University Grants Commission (MRP-MAJOR-ELEC-2013-37628) and RUSA 2.0 [F.24–51/2014-U, Policy (TN Multi-Gen), Dept of Edn, Gol] for financial assistance.

Appendix A. Supplementary data

Supplementary data to this article can be found online at https://doi.org/10.1016/j.bcab.2019.101352.

References

Ahammad, A.J.S., et al., 2011. Highly sensitive and simultaneous determination of hydroquinone and catechol at poly(thionine) modified glassy carbon electrode. Electrochim. Acta 56, 5266–5271.
Ali, A., et al., 2012. Fabrication of DNA, o-phenylenediamine, and gold nanoparticle bioimprinted polymer electrochemical sensor for the determination of dopamine Biosens. Bioelectromagnetics 31, 376–381.
Ansari, A.A., et al., 2008. Sol-gel derived nanostructured cerium oxide film for glucose sensor. Appl. Phys. Lett. 92, 263–901.
Becerra-Herrera, M., et al., 2014. Determination of phenolic compounds in olive oil: new method based on liquid–liquid micro extraction and ultra high performance liquid chromatography-triple–quadrupole mass spectrometry. Food Sci. Technol. 57, 49–57.
Berti, L., et al., 2005. Intramolecular Diels−Alder reactions of optically active allenic Ketones: chirality transfer in the preparation of substituted oxa-bridged octalones. J. Am. Chem. Soc. 127, 11216–11217.
Bhandari, R., et al., 2013. Structural control and catalytic reactivity of peptide-templated Pd and Pt nanomaterials for olefin hydrogenation. J. Phys. Chem. C 35 (117), 18053–18062.
Chang, K., et al., 2015. An advanced MoS 2/carbon anode for high-performance sodium-ion batteries. J. Mater. Chem. 4 (11), 473–481.
He, J., et al., 2012. Development of a cloud point extraction method for the determination of phenolic compounds in environmental water samples coupled with high-performance liquid chromatography. Separ. Sci. 35, 1003–1009.
Huang, Y.H., et al., 2015. One-pot hydrothermal synthesis carbon nanocages-reducegraphene oxide composites for simultaneous electrochemical detection of catechol and hydroquinone. Sens. Actuators B Chem. 212, 165–173.
Ji, T., et al., 2016. Thermal conducting properties of aligned carbon nanotubes and their polymer composites. Composites, Part A 91, 351–369.
Jiménez-Monroy, K.L., et al., 2017. High electronic conductance through double-helix DNA molecules with fullerene anchoring groups. J. Phys. Chem. A 121, 1182–1188.
Keren, K., et al., 2013. Molecular motions in functional self-assembled nanostructures. Science 2 (14), 2303–2333.
Kundu, S., et al., 2013. Bioinspired synthesis of Ag@TiO2 plasmonic nanocomposites to enhance the light harvesting of dye-sensitized solar cells. Langmuir 40 (3), 18587–18595.
Lee, S.W., et al., 2002. Ordering of quantum dots using genetically engineered viruses. Science 5569 (296), 892–895.
Li, Y., et al., 2014. Recent advances in graphene based gas sensors. Sens. Actuators, B 205, 227–233.
Li, W., et al., 2017. A catalytic assembled enzyme-free three-dimensional DNA walker and its sensing application. Chem. Commun. 53, 5527–5530.
Liang, S.Q., et al., 2013. PVP-assisted synthesis of MoS2 nanosheets WithImproved lithium storage properties. CrystEngComm 25 (15), 4998–5002.
Liao, C.I., et al., 2012. Acetylcholinesterase liquid crystal biosensor based on modulated growth of gold nanoparticles for amplified detection of acetylcholine and inhibitor. Anal. Chem. 84, 7440–7448.
Lim, D.K., et al., 2010. Nanogap-engineerable Raman-active nanodumbbells for single-molecule detection. Nat. Mater. 1 (9), 60–67.
Liu, J., et al., 2010. Tin oxide nanorod array-based electrochemical hydrogen peroxide biosensor. Nanoscale Res. Lett. 5, 1177–1181.
Lu, Q., et al., 2014. One-pot hydrothermal synthesis of amine-functionalized metal-Organic framework/reduced graphene oxide composites for the electrochemical detection of bisphenol A. Biosens. Bioelectron. 60, 325–331.
Lv, M., et al., 2010. Electrochemical detection of catechol based on as-grown and nanograss array boron-doped diamond electrodes. Electroanalysis 22, 199–203.
Maiyalagan, T., et al., 2013. Nanostructured α-Fe_2O_3 platform for the electrochemical sensing of folic acid. Analyst 6 (138), 1779–1786.
Matte, H.S.S.R., et al., 2010. MoS2 and WS2 analogues of graphene. Chem. Int. Ed. 24, 4059–4062.
Medina-Plaza, C., et al., 2015. Self-Assembled patterns and young's modulus of single-layer naphthalocyanine molecules on Ag(111). J. Phys. Chem. C 119, 25100–25107.
Miao, P., et al., 2017. DNA modified Fe3O4@Au magnetic nanoparticles as selective probes for simultaneous detection of heavy metal ions. ACS Appl. Mater. Interfaces 9, 3940–3947.
Mirkin, C.A., et al., 2000. Programming the assembly of two- and three-dimensional architectures with DNA and nanoscale inorganic building blocks inorg. Chem 39, 2258–2272.
Mittal, G., et al., 2015. A review on carbon nanotubes and graphene as sellers in reinforced polymer nanocomposites. J. Ind. Eng. Chem. 21, 11–25.
Munir, A., et al., 2017. Microwave radar absorbing properties of multiwalled carbon nanotubes polymer composites:a review. Adv. Polym. Technol. 36, 362–370.
Nagaraja, P., et al., 2001. Electrocatalytic oxidation and simultaneous determination of catechol and hydroquinone at a novel carbon nano-fragment modified glassy carbon electrode. Talanta 55, 1039–1046.
Nimbalkar, D.B., et al., 2016. Stable dispersed MoS2 nanosheets in liquid lubricant with enhanced rate of penetration for directional well. RSC Adv. 8, 31661–31667.
Pramanik, C., et al., 2018. Molecular engineering of interphases in polymer/carbon nanotube composites to reach the limits of mechanical performance. Compos. Sci. Technol. 166, 86–94.
Prusty, R.K., et al., 2017. CNT/polymer interface in polymeric composites and its sensitivity study at different environments. Adv. Colloid Interface Sci. 240, 77–106.
Rahmat, M., et al., 2017. Carbon nanotube-polymer interactions in nanocomposites: a review. Compos. Sci. Technol. 72, 72–84.
Seidel, R., et al., 2004. DNA as a selective metallization template. J. Phys. Chem. B 108, 10801–10811.
Sevilla, M., et al., 2014. Classification of carbon materials for developing structure-properties relationships based on the aggregatestate of the precursors. Chin. J. Catal. 6 (35), 778–782.
Soon, J.M., et al., 2011. Electrochem. Electrochemical double-layer capacitance of MoS_2 nanowall films. Solid-State Lett. 10, 250–254.
Sumathi, C., et al., 2015. Riboflavin detection by α-Fe_2O_3/MWCNT/AuNPs-based composite and a study of the interaction of riboflavin with DNA. RSC Adv. 5, 17888–17896.
Sumathi, C., et al., 2016. Au–Pd bimetallic nanoparticles anchored on α-Fe_2O_3 nonenzymatic hybrid nanoelectrocatalyst for simultaneous electrochemical detection of dopamine and uric acid in the presence of ascorbic acid. J. Mater. Chem. B. 4, 2561–2569.
Umare, S.S., et al., 2018. Synthesis and characterization of polyaniline-Fe3O4 Na-nocomposite: electrical Conductivity,Magnetic, electro-chemical studies. Synth. Met. 18, 1815–1821.
Vyborna, Y., et al., 2017. Functional DNA-grafted supramolecular polymers– chirality, cargo binding and hierarchical organization. Chem. Commun. 53, 5179–5181.
Wang, H., et al., 2015. Dispersed gold nanoparticles on NiO coated with polypyrrole for non- enzymic amperometric sensing of glucose. Sens. Actuators B 220, 749–754.
Yan, X.B., et al., 2010. Fabrication of free-standing, electrochemically active, and biocompatible graphene Oxide−Polyaniline and Graphene−Polyaniline hybrid papers. Appl.Mater. Interfaces. 2, 2521–2529.
Yan, L., et al., 2017. MoS2-DNA and MoS2 based sensors. RSC Adv. 7, 23573–23582.
Yang, C.C., et al., 2010. Graphene decorated with hexagonal shaped M-type ferrite and polyaniline wrapper: a potential candidate for electromagnetic wave absorbing and energy storage device applications. Magn.Mater. 323, 933–938.
Zahedi, M., et al., 2017. Spectrophotometric monitoring of nitrite in seawater after liquid microextraction of its derivative with 2, 3-diaminonaphthalene. Water Qual Res J 52, 11–17.
Zhou, X.S., et al., 2012. Facile synthesis of MoS2@ CMK-3 nanocomposite as an improved anode material for lithium- ion batteries. Nanoscale 19 (4), 5868–5871.